Structural and electronic properties of crystalline and glassy calcium-zinc compounds. I. Trigonal prismatic ordering or tetrahedral close packing

1989 J. Phys.: Condens. Matter 1 8277

(http://iopscience.iop.org/0953-8984/1/44/001)

J. Phys.: Condens. Matter **1** (1989) 8277–8291. Printed in the UK

Structural and electronic properties of crystalline and glassy calcium–zinc compounds: I. Trigonal prismatic ordering or tetrahedral close packing

J Hafner and M Tegze†
Institut für Theoretische Physik, Technische Universität Wien,
Wiedner Hauptstrasse 8–10, A-1040 Wien, Austria

Received 29 March 1989

Abstract. We present a detailed molecular dynamics study of the atomic structure of liquid and amorphous Ca–Zn alloys, based on inter-atomic forces derived from optimised first-principles pseudopotentials. In the Zn-rich limit, our results fit into the pattern characteristic for other simple-metal alloys; the liquid and the quench-condensed amorphous phase can be described as disordered tetrahedrally close packed. For the Ca-rich phases we find some distinctly different features; the most prominent is a pre-peak in the partial structure factor $S_{Zn-Zn}(q)$ and in the number-density structure factor $S_{NN}(q)$, indicating topological short-range order. The analysis of the bond distances, coordination numbers and bond angles shows that the local order might be described as trigonal prismatic (distorted trigonal prisms of Ca, centred by Zn), in analogy to the trigonal prismatic structures of the crystalline inter-metallic compounds Ca_3Zn(Re_3B-type), Ca_5Zn_3(Cr_5B_3 type) and CaZn(CrB type).

1. Introduction

It has been pointed out some time ago that in many alloy systems there is a remarkable coincidence between the formation of glassy alloys and the formation of certain classes of stoichiometric crystalline inter-metallic compounds [1, 2]. For example the crystalline borides, phosphides, silicides, etc, of those transition metals which readily form metallic glasses with boron, phosphorus or silicon have structures based on a trigonal prismatic coordination of the metalloid by the transition-metal atoms. This characteristic local unit persists over a wide range of compositions (including the glass-forming composition) and over a range of radius ratios differing widely from the ideal radius ratio for an undistorted trigonal prism. Thus this type of local topology seems to be especially stable. This has led to the proposal [3, 4] that, in modelling the structure of the glassy phase, one should proceed by a random packing of these trigonal prismatic units rather than of individual atoms as these groups of atoms seem to possess advantageous energetic or space-filling properties. Later it was shown [5] that indeed computer-generated models for transition-metal–metalloid glasses possess a large degree of trigonal prismatic order and that this is a consequence of the atomic size difference and a strong short-range interaction between the metal and the metalloid atoms. However, up to now it has not been possible to derive these inter-atomic potentials from an electronic theory of the chemical bond.

† On leave of absence from Central Research Institute for Physics, Hungarian Academy of Sciences, PO Box 49, H-1525 Budapest, Hungary.

0953-8984/89/448277 + 15 $02.50

On the contrary, the glasses formed by simple metals (e.g. Mg–Zn, Ca–Mg, Ca–Al), by simple metals with transition metals (Ti–Be, Zr–Be, etc.), by simple metals with rare-earth metals (La–Al, La–Ga, etc.), and by transition- and rare-earth metals (Gd–Co, Tb–Fe, etc.) are closely related to tetrahedrally close-packed crystalline inter-metallic phases [6]. Their phase diagrams are characterised by very stable (congruently melting) Laves phases or Frank–Kasper phases at majority concentrations of the smaller atoms. Metallic glasses are formed at majority concentrations of the larger atoms. The glass-forming region extends around a deep eutectic minimum. At these compositions there are usually no or only a few relatively unstable compounds with very complex structures (among the few exceptions are the Mg_2Cu and $CuAl_2$ phases). Unifying features of the stable structures are the principle of tetrahedral close packing and coordination in the form of certain triangulated polyhedra [7]. The smaller majority atoms have a coordination number N_c of 12; the coordination polyhedron is an eventually distorted icosahedron. The icosahedra are linked by inter-penetrating Kasper–Friauf polyhedra with very large coordination numbers (N_c = 16, 18, 20, 22 or 24) [8–10]. The quasi-omnipresence of icosahedral coordination is at least indicative of possible local motifs in the amorphous structures. This has led to a Ginzburg–Landau description for the structure and the statistical mechanics of short-range icosahedral order in supercooled liquids and glasses [11, 12]. A high degree of icosahedral order has also been found in molecular dynamics simulations for a number of Mg- and Ca-based simple metal glasses [13–16]. For these simple-metal glasses the inter-atomic potentials can be deduced from *ab initio* pseudopotentials and linear response theory [17, 18]. A detailed investigation of the partial structure factors, pair correlation functions and bond angle distribution functions shows that as in the tetrahedrally close-packed crystalline compounds the smaller atoms in the glass have an environment with icosahedral symmetry, while the surroundings of the larger atoms have the symmetry of the Kasper–Friauf polyhedra. The conclusion that the local order in the glasses is similar to that in the intermetallic compounds is further supported by electronic structure calculations and the comparison of the results with photoemission and x-ray emission spectroscopy [13–16].

In this paper we present the results of detailed investigations of the structural properties of crystalline and amorphous Ca–Zn alloys. The Ca–Zn system has a very complex phase diagram (figure 1). Eight inter-metallic phases are known and have been fully characterised [8, 9] (tables 1–5). The three phases richest in Zn are based on large coordination polyhedra with mostly triangular and only a few square faces and on Kasper–Friauf polyhedra; $CaZn_5$ is a genuine tetrahedrally close-packed Frank–Kasper phase (figure 2). All these phases are very stable; their melting points are much higher than the concentration averages of the melting points of the pure metals. The four compounds richest in Ca are based on the packing of trigonal prisms. In Ca_3Zn the trigonal Ca_6 prisms centred by a Zn atom are arranged in columns running parallel to the *a* axis (figure 3(*a*)). In CaZn the trigonal prisms form layers, the Zn atoms within each layer forming zigzag chains (figure 3(*b*)). These two structures—and the structure of Ca_5Zn_3—are also found in many transition-metal borides. The $CaZn_2$ structure may be viewed as a close-packed arrangement of slightly distorted trigonal prisms in three dimensions (figure 3(*c*)). The trigonal prismatic phases have a rather modest stability. The liquidus curve has a very deep eutectic minimum (the melting point is depressed by 22% relative to the concentration average!), and all the three compounds richest in Ca decompose peritectically. Metallic glasses are formed at Ca concentrations of between 80 and 40 at.% [1, 27].

It is an open question whether the structure of the Ca–Zn glasses is best described as a disordered tetrahedral close packing—like all the other simple-metal glasses—or

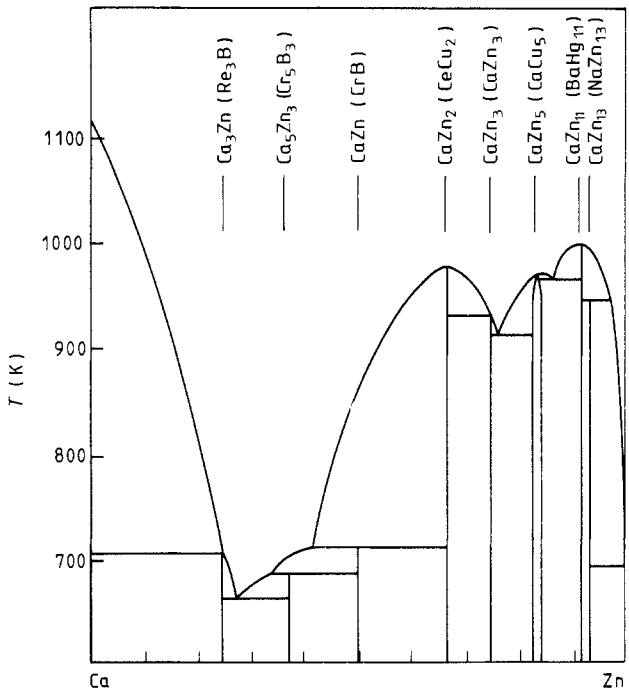

Figure 1. Ca–Zn phase diagram (schematically after [19–21]). The structure of each phase is given in parentheses.

Table 1. Inter-metallic phases in the Ca–Zn system.

Phase	Symmetry symbol	Structure type	Volume of formation (%)	Reference
$CaZn_{13}$	cF112	$NaZn_{13}$	−5.8	[8]
$CaZn_{11}$	tI48	$BaCd_{11}$	−6.8	[8]
$CaZn_5$	hP6	$CaCu_5$	−10.6	[9]
$CaZn_3$	hP32	$CaZn_3$	−10.7	[22]
$CaZn_2$	oI12	$CeCu_2$	−12.4	[23]
CaZn	oC8	CrB	−7.6	[21, 24]
Ca_5Zn_3	tI32	Cr_5B_3	−7.0	[25]
Ca_3Zn	oC16	Re_3B	−3.8	[21, 24]

Table 2. Crystallographic data of the $CaZn_5$ phase.

Space group D^1_{6h}

$a = 5.416$ Å
$c = 4.191$ Å $\quad c/a = 0.7738$

Atomic positions

Ca	(1a)	0	0	0
Zn(1)	(2c)	$\frac{1}{3}$	$\frac{2}{3}$	0
Zn(2)	(3g)	$\frac{1}{2}$	0	$\frac{1}{2}$

Coordination

	Ca	Zn(1)	Zn(2)	Zn	Total
Ca	2	6	12	18	20
Zn(1)	3	3	6	9	12
Zn(2)	4	4	4	8	12

Inter-atomic distances (Å)

d_{Ca-Ca}	4.19
d_{Ca-Zn}	3.12–3.42
d_{Zn-Zn}	2.61–3.12

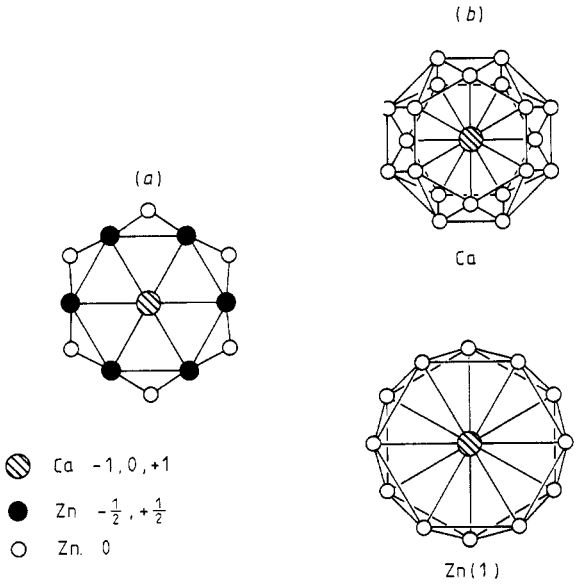

Figure 2. Coordination polyhedra around Ca atoms and Zn atoms in (*a*) $CaZn_5$ and (*b*) $CaZn_{11}$, projected along the *c* axis. (After [10].)

Table 3. Crystallographic description of the $CaZn_2$ phase.

Space group D_{2h} [26]				Atomic positions				
$a = 4.591$ Å				Ca	(4e)	0	$\frac{1}{4}$	0.553
$b = 7.337$ Å	$b/a = 1.5981$			Zn	(8h)	0	0.057	0.165
$c = 7.667$ Å	$c/a = 1.6700$							
Coordination				Inter-atomic distances (Å)				
	Ca	Zn	Total	d_{Ca-Ca}	3.76–3.84,	4.59,	5.18	
Ca	4 + 2(+2)	12	16 + 12(+2)	d_{Ca-Zn}	3.12–3.33			
Zn	6	4	10	d_{Zn-Zn}	2.64–2.83			

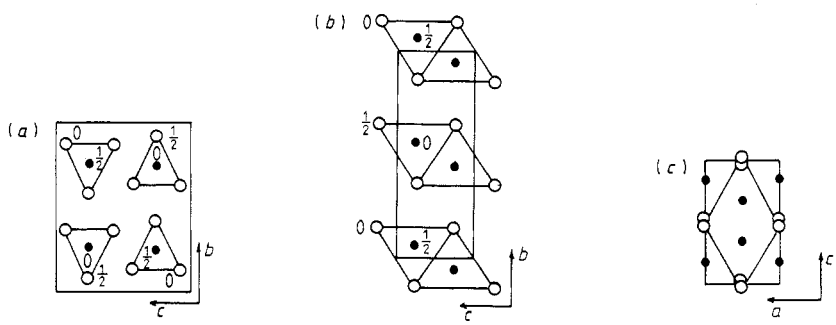

Figure 3. The unit cells of the trigonal prismatic phases (*a*) Ca_3Zn, (*b*) CaZn and (*c*) $CaZn_2$. (After [10].)

Table 4. Crystallographic description of the CaZn phase.

Space group D_{2h} [17]				Atomic positions				
$a = 4.202$ Å				Ca	(4c)	0	0.145	$\frac{1}{4}$
$b = 11.61$ Å	$b/a = 2.763$			Zn	(4c)	0	0.435	$\frac{1}{4}$
$c = 4.402$ Å	$c/a = 1.057$							
Coordination				Inter-atomic distances (Å)				
	Ca	Zn	Total	d_{Ca-Ca}	3.91–4.44			
Ca	10	7	17	d_{Ca-Zn}	3.19–3.30			
Zn	7	2	9	d_{Zn-Zn}	2.68			

Table 5. Crystallographic description of the Ca_3Zn phase.

Space group D_{2h} [17]						Atomic positions				
$a = 4.150$ Å						Ca(1)	(4c)	0	0.4323	$\frac{1}{4}$
$b = 13.26$ Å	$b/a = 3.19$					Ca(2)	(8f)	0	0.1414	0.0605
$c = 10.19$ Å	$c/a = 2.45$					Zn	(4c)	0	0.7524	$\frac{1}{4}$
Coordination						Inter-atomic distances (Å)				
	Ca(1)	Ca(2)	Zn	Ca	Total	$d_{Ca-Ca} = 4.19,$	5.41			
Ca(1)	2	10	2 + 1	12	14 + 1	$d_{Ca-Zn} = 3.12–3.42,$	5.13			
Ca(2)	5	6	3	11	14	$d_{Zn-Zn} = 2.61–3.12,$	4.19			
Zn	2 + 1	6	0 + 1	8 + 1	8 + 3					

whether the local order is dominated by the same trigonal prismatic units as in the Ca-rich crystalline compounds. Here we present detailed molecular dynamics investigations of liquid and amorphous alloys at four different compositions chosen to coincide with three of the trigonal prismatic compounds (Ca_3Zn, CaZn and $CaZn_2$) and with the Frank–Kasper phase $CaZn_5$. In the second paper of this series the investigation of the atomic structure will be supplemented by detailed calculations of the electronic structure for the crystalline and the amorphous phases.

2. Inter-atomic potentials

Our method for calculating inter-atomic forces in metals and alloys on the basis of pseudopotentials and linear response theory has been well documented elsewhere [2, 15, 18]. There we have emphasised that the variation in the optimised non-local ionic pseudopotential with composition is important for describing the alloying effects on the inter-atomic interactions. In strong-scattering heterovalent alloys such as Ca–Al [15] or K–Pb [28] the variation in the ionic pseudopotential and the change in the electron gas susceptibility individually both have a large, and to some extent mutually compensating, influence on the inter-atomic potentials. The situation is different in homovalent systems with a large difference in the atomic volumes of the constituent metals; as the ionic charge is the same, the variation in the ionic pseudopotentials will be small. However, as the electron density changes by a factor of nearly 3 across the series, the change in the susceptibility will lead to a rather pronounced variation in the inter-atomic potentials. This is illustrated in figure 4 where we show the inter-atomic potentials at four different compositions, calculated using a composition-independent local empty-core model

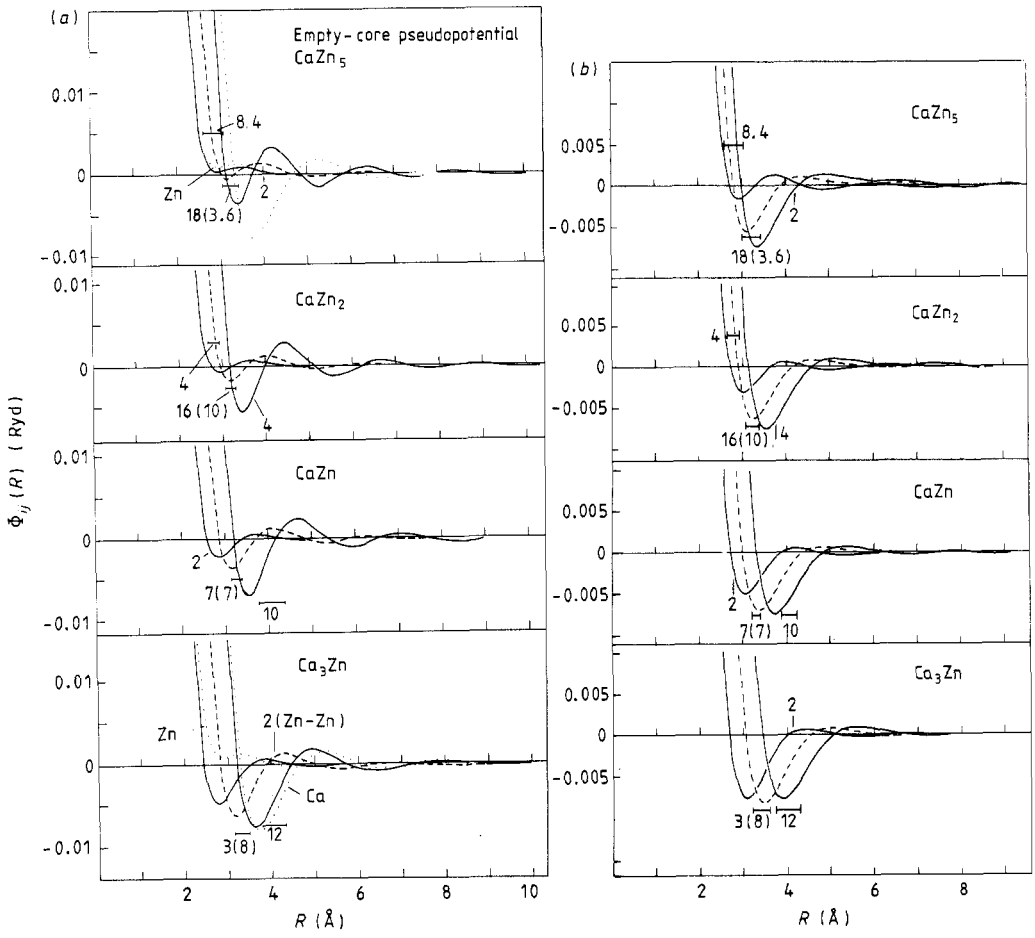

Figure 4. Inter-atomic potentials in four Ca–Zn phases calculated using (*a*) the local composition-independent empty-core pseudopotential and (*b*) the non-local optimised pseudopotential (see text): ——, Ca–Ca and Zn–Zn interactions in the alloy; ---, Ca–Zn potentials; ····, pair potentials in pure Ca and Zn. The nearest-neighbour distances in the inter-metallic compounds and the coordination numbers are indicated (for unlike-atom coordinations the first number refers to Zn atoms around Ca, and the number in parentheses to Ca atoms around Zn), averaged over crystallographically inequivalent positions. Note that the shortest Ca–Ca distances indicated for $CaZn_5$ and the shortest Zn–Zn distances given for Ca_3Zn do not represent direct neighbours.

potential (the core radii $R_c(Ca) = 0.92$ Å and $R_c(Zn) = 0.56$ Å have been chosen so as to fit the lattice parameters of the pure metals [18]), and using a non-local pseudopotential optimised specifically for each composition of the alloy [18]. For these homovalent alloys the resulting inter-atomic potentials derived from the different pseudopotentials are in reasonable agreement, except for small differences in the oscillatory part of the potentials.

The change in the susceptibility as a function of the valence electron density accounts for the largest effect. As a consequence of the change in the Fermi momentum k_F, the wavelength λ_F of the Friedel oscillations will be smaller in the Ca–Zn alloy than in pure Ca. With the empty-core form of the pseudopotential, the effective repulsive diameter of the pair interaction is given by [18, 26] $D_r^i = 2R_c^i + 2\lambda_F$. Hence the effective diameter

of the Ca atoms will decrease and that of the Zn slightly increase on alloying. The second effect is the change in the on-Fermi-surface matrix element of the pseudopotential setting the amplitude of the Friedel oscillations. Quite generally a reduced electron density leads to an increase in the amplitude of the Friedel oscillations, because the screening is less effective. As far as the effective diameter of the atoms is concerned, this effect goes against the shift of the Friedel oscillations. Hence altogether the effective size of the Zn atoms is hardly affected on alloying, while there remains a small compression of the Ca atoms. For the pure metals we deduce an effective radius ratio R_{Ca}/R_{Zn} of about 1.40 from the positions of the first minima in the pair potentials calculated with the non-local pseudopotential. This value is close to the ratio of the Goldschmidt radii.

The effective inter-atomic potentials shown in figure 4 are almost additive in the sense that

$$\Phi_{Ca\text{-}Zn}(d_{Ca\text{-}Zn}) \simeq \tfrac{1}{2}[\Phi_{Ca\text{-}Ca}(d_{Ca\text{-}Ca}) + \Phi_{Zn\text{-}Zn}(d_{Zn\text{-}Zn})]$$

where d_{ij} is the nearest-neighbour distance. The pair interactions derived from the non-local pseudopotentials show a slight preference for the formation of unlike-atom pairs, and those derived from the empty-core model potentials rather a slight tendency for the formation of like-atom pairs (at least in the Zn-rich alloys). The pair interactions in any case do not show the strong preference for the formation of unlike-atom pairs suggested by the total absence of Zn–Zn nearest-neighbour pairs in Ca_3Zn, of Ca–Ca nearest neighbours in $CaZn_5$ and of the predominance of unlike atom pairs in the remaining compounds. If the potentials are compatible with the observed local order (and there is no evident reason why a method for constructing inter-atomic potentials that works well for Ca–Mg and Ca–Al [14, 15] should fail for Ca–Zn), its origin must be influenced largely by steric effects.

3. Molecular dynamics simulations of liquids and glasses

In our previous studies of the structural and electronic properties of metallic glasses [13–16] we have used a molecular dynamics simulation linked to a steepest-gradient potential energy mapping. The potential energy mapping consists in the projection of independent instantaneous configurations of the liquid onto local potential energy minima via a steepest-gradient descent on the potential energy surface. It has been shown [13, 29, 30] that the correlation functions obtained by averaging over a number of local configurations belonging to different potential energy minima are independent of the thermodynamic state of the system before the mapping; hence they really represent the 'inherent' structure of the liquid. The actual structure of the liquid is the result of thermally induced distortions of this locally stable structure. The inherent structure of the liquid is found to be a very realistic model for the glassy structure; it depends only on the inter-atomic forces and is independent of the thermal history of the sample which is important for the result of real as well as simulated quench experiments.

This last point could be problematic for the simulation of Ca–Zn glasses; in the crystalline compounds we find two distinct classes of inter-metallic compounds and we suspect that eventually there are also two different regimes of local order in the liquid as a function of composition. It is certainly not impossible that the boundary between these two regimes shifts with temperature. Therefore we decided to proceed entirely by molecular dynamics in the following way: in a first run the crystalline starting configuration is molten at a high temperature, in the second run the temperature is slowly

lowered to a value not too far above the liquidus and equilibrated at this temperature, and in a third run the data for calculating correlation functions are sampled. All three runs are performed at the density of the liquid alloy at the measuring temperature. Glasses are produced by first compressing the high-temperature liquid alloy isothermally to the density of the glass (taken to be identical with that of the intermetallic compound) and equilibrated. In the next run the temperature is reduced step by step to room temperature, the effective cooling rate being $T \simeq 10^{14}\,\mathrm{K\,s^{-1}}$, followed by another equilibration run. In a final run, data for the glassy configurations are sampled.

Details of our microcanonical constant-energy molecular dynamics routine have been given elsewhere [31, 32]; we use a fifth-order predictor–corrector algorithm for the integration of the equations of motion (this permits us to keep the energy constant to within five significant digits at a time increment Δt of 0.3×10^{-14} s) and an efficient link cell method for neighbour book-keeping (with this method the computer time increases only linearly with the number of atoms per cell; thus simulations of quite large models are possible).

All our simulations are performed for 1372 atoms in a periodically repeated cell. The oscillatory potentials are cut off at a node of the pair potential situated at a distance corresponding to about 30% of the edge of the molecular dynamics cell ($R_{\mathrm{cut}} \simeq 17$–$22$ Å). With this choice of the cut-off, each atom interacts on the average with 150–160 neighbours. With a time increment Δt of about 0.3×10^{-14} s, typical equilibration runs (after melting and after first reaching the desired temperature, respectively) take 1500–2000 time steps, cooling runs 3000–5000 time steps, and production runs 1000 steps, with data sampled every tenth step (i.e. a typical correlation function is based on the average over 100 independent configurations).

4. Structure of liquid and amorphous Ca–Zn alloys

In the following we compare the atomic structure of four different liquid and amorphous Ca–Zn alloys (as characterised by the partial pair correlation functions $g_{ij}(R)$ (figure 5), the structure factors $S_{ij}(q)$ (figure 6), and the bond angle distribution functions $f(\theta)$ (figure 7)) with the structure of the stable crystalline compounds. Two of these alloys ($CaZn_5$ and $CaZn_2$) cannot be produced in amorphous form in the laboratory. At the much higher quenching rate of the computer experiment, however, an amorphous phase is readily formed.

4.1. $CaZn_5$

The partial pair distribution functions of liquid and quenched $CaZn_5$ are shown in figure 5(*a*). The shortest Zn–Zn and Ca–Zn distances correspond rather well to the nearest-neighbour distances in the Frank–Kasper phase, but the shortest Ca–Ca distances are considerably compressed. The total and partial coordination numbers calculated by integration over the first peak of the radial distribution function up to the first minimum in the relevant $g_{ij}(R)$ are compiled in table 6—but note that this definition of a nearest neighbour is not exactly the same as that used in crystallography. This is the reason for the much lower coordination number of the Ca atoms in the amorphous phase compared with the crystal. Otherwise the coordination numbers are in reasonable agreement. In the glass and in the crystal we find a slight preference for the formation of unlike-atom pairs but, as expected, this chemical short-range order (CSRO) is weaker in the amorphous

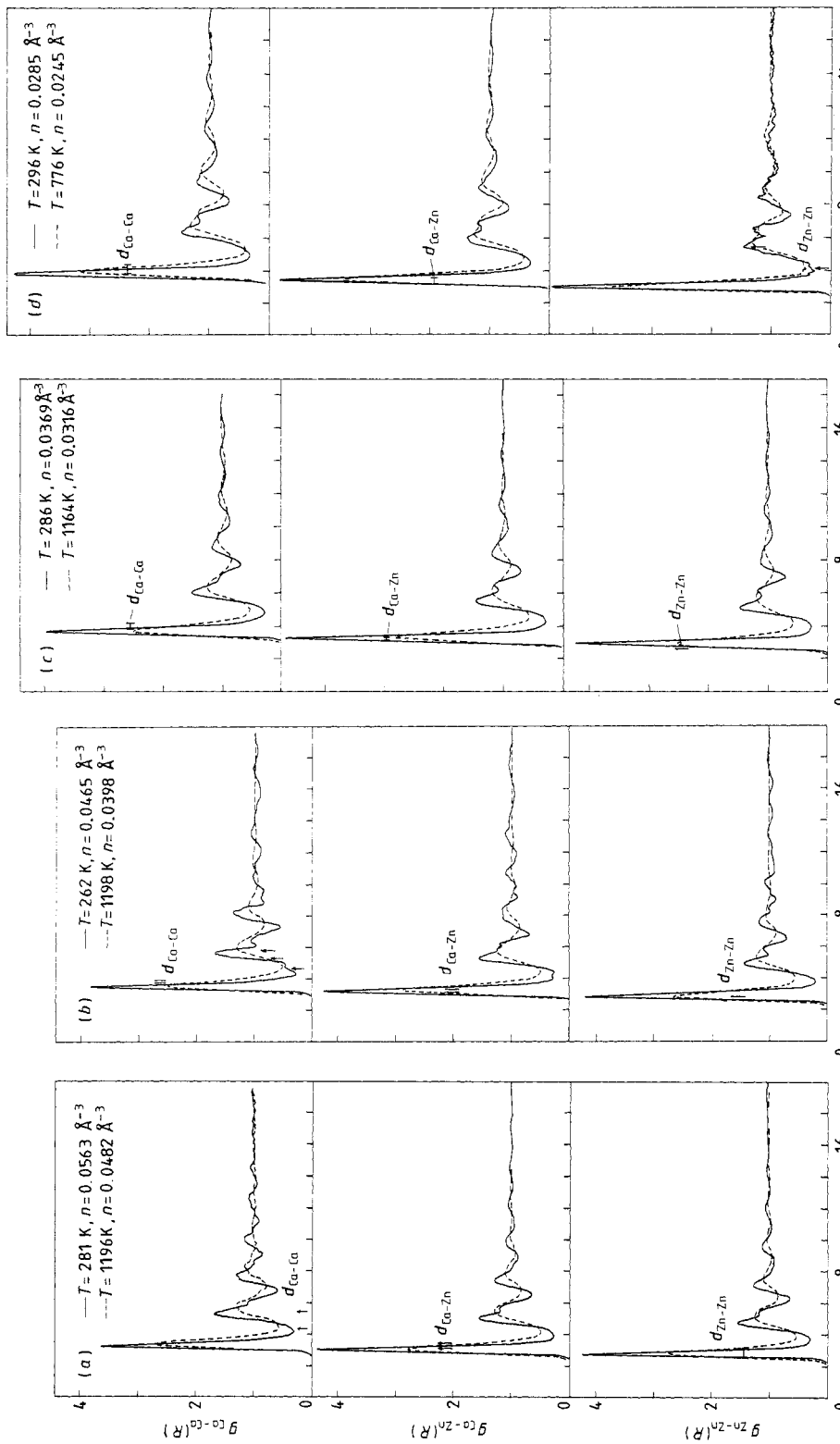

Figure 5. Partial pair correlation functions $g_{ij}(R)$ in liquid (——) and amorphous (— — —) Ca_xZn_{1-x} alloys: (*a*) $CaZn_5$; (*b*) $CaZn_2$; (*c*) CaZn; (*d*) Ca_3Zn. The nearest- and next-nearest neighbour distances are indicated.

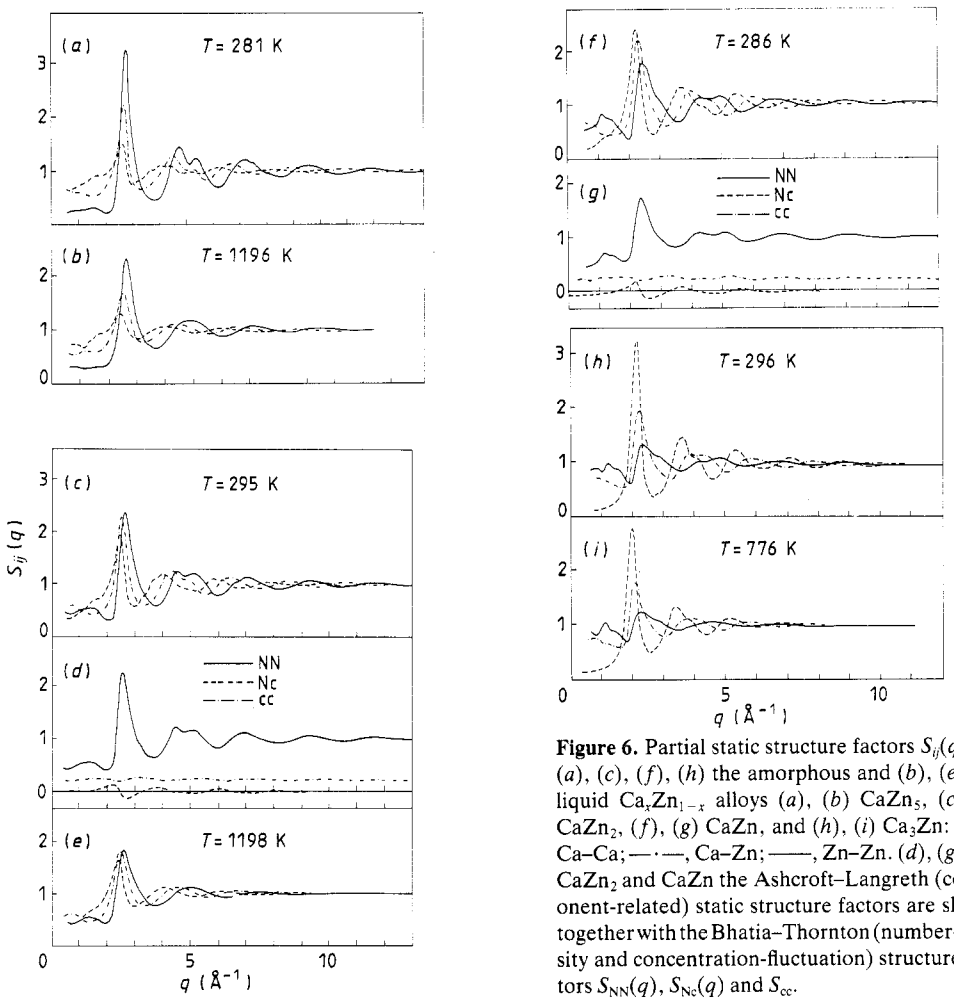

Figure 6. Partial static structure factors $S_{ij}(q)$ for (*a*), (*c*), (*f*), (*h*) the amorphous and (*b*), (*e*), (*i*) liquid Ca_xZn_{1-x} alloys (*a*), (*b*) $CaZn_5$, (*c*)–(*e*) $CaZn_2$, (*f*), (*g*) CaZn, and (*h*), (*i*) Ca_3Zn: ---, Ca–Ca; —·—, Ca–Zn; ——, Zn–Zn. (*d*), (*g*) For $CaZn_2$ and CaZn the Ashcroft–Langreth (component-related) static structure factors are shown together with the Bhatia–Thornton (number-density and concentration-fluctuation) structure factors $S_{NN}(q)$, $S_{Nc}(q)$ and S_{cc}.

phase. The partial structure factors (figures 6(*a*) and 6(*b*)) and bond angle distributions (figure 7(*a*)) are very similar to those found in other quench-condensed Franz–Kasper alloys (e.g. quenched $MgZn_2$ [16]); we find a structure factor with a very sharp first and a split second peak for the small majority atoms (Zn), and an asymmetric broad peak for the large minority atoms. The distribution of the bond angles centred at the Zn atoms (in the following, $f_i(\theta)$, i ≡ Ca, Zn, stands for the distribution of the bond angles centred at a site of type i, irrespective of its nearest neighbours) shows two sharp peaks situated close to the icosahedral bond angles ($\theta = 63.5°$ and $\theta = 116.5°$)—this points to a predominantly icosahedral symmetry of the environment of the Zn atoms in the amorphous phase, as in the crystal. The distribution of the angles formed by bonds centred at the Ca sites has three peaks; compared with $f_{Zn}(\theta)$ the first two peaks are shifted to smaller angles, and the third peak lies at $\theta \simeq 145°$. Again this is similar to other amorphous simple-metal phases such as Mg–Zn. The crystalline phase shows the same three-peaked $f_{Ca}(\theta)$, but the main peaks occur at even smaller bond angles. The origin of this difference is in the somewhat greater Ca–Zn bond length. Altogether this hypothetical amorphous $CaZn_5$ can be characterised as disordered tetrahedrally close packed in analogy to the glassy Ca–Mg and Mg–Zn phases.

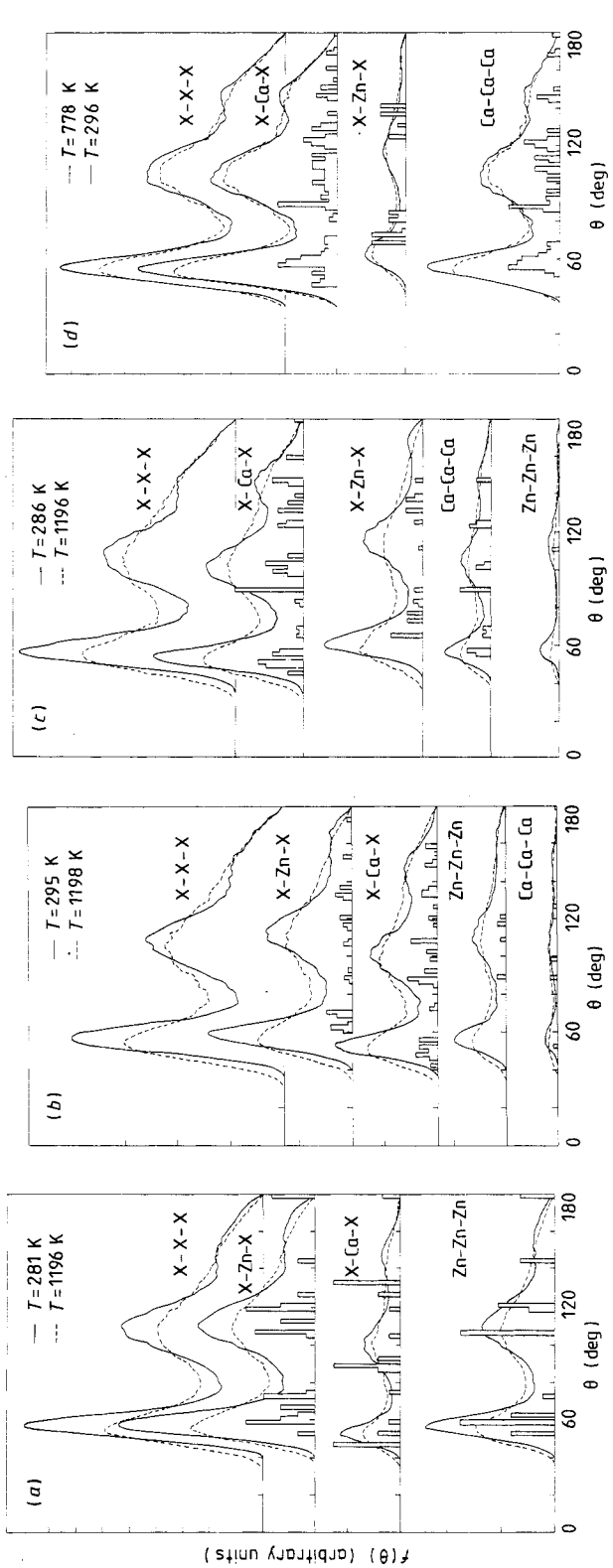

Figure 7. Bond angle distributions in liquid (——) and amorphous (– – –) Ca_xZn_{1-x} alloys: (*a*) $CaZn_5$; (*b*) $CaZn_2$; (*c*) CaZn; (*d*) Ca_3Zn. The histograms show for comparison the bond angles in the crystalline inter-metallic compound. Whenever necessary, an average over crystallographically inequivalent sites has been taken.

Table 6. Coordination numbers in crystalline and glassy Ca–Zn alloys

	Ca total	Ca	Zn	Zn total	Zn	Ca
Ca_3Zn crystal[a]	14	11.3	2.7	8	0	8
		(10.5)	(3.5)[b]		(2.0)	(6.0)
Ca_3Zn glass	14.0	11.2	2.8	10.3	2.0	8.3
		(10.5)	(3.5)		(2.6)	(7.7)
CaZn crystal[a]	17	10	7	9	2	7
		(8.5)	(8.5)		(4.5)	(4.5)
CaZn glass	14.5	8.0	6.5	11.1	4.5	6.5
		(7.25)	(7.25)		(5.55)	(5.55)
$CaZn_2$ crystal[a]	16	4	12	10	4	6
		(5.3)	(10.7)		(6.7)	(3.3)
$CaZn_2$ glass	14.7	5.2	9.5	11.8	7.2	4.6
		(4.8)	(9.9)		(7.9)	(3.9)
$CaZn_5$ crystal[a]	20	2	18	12.0	8.4	3.6
		(3.3)	(16.7)		(10.0)	(2.0)
$CaZn_5$ glass	14.7	2.5	12.2	12.2	9.7	2.5
		(2.4)	(12.3)		(10.2)	(2.0)

[a] Coordination numbers are weighted averages over crystallographically inequivalent sites.
[b] The numbers in parentheses give the partial coordination numbers for a chemically random alloy at a fixed total coordination number for each species.

4.2. $CaZn_2$

Unlike the homologous compounds $CaMg_2$ and $CaCd_2$ which form hexagonal Laves phases with the C14 ($MgZn_2$-type) structure, $CaZn_2$ assumes the $CeCu_2$ structure (see table 1). The reason is clearly the much larger radius ratio of the two components. Owing to the alloying effects the effective size ratio is somewhat reduced compared with the pure metals, but unlike the situation for $CaAl_2$ the reduction is not strong enough to stabilise a Laves phase.

The partial pair correlation functions $g_{ij}(R)$ are shown in figure 5(b). Again we find a distinct tendency to smaller Ca–Ca distances than in the crystal, whereas Ca–Zn and Zn–Zn distances are the same in both phases. The positions of the maxima of the split second peak corresponds about equally well to the second- and third-neighbour distances in the Laves phases or in the $CeCu_2$ phase. As in the Laves phases, the formation of unlike-atom pairs is strongly preferred in the crystalline structure. There are no Zn–Zn bonds forming angles close to 60° as the CSRO suppresses the formation of Zn-nearest-neighbour triplets (see also figure 3(c)). However, as the CSRO is much weaker, such triplets exist in the amorphous phase and the general form of $f_{Zn}(\theta)$ and $f_{Ca}(\theta)$ is not so different from that in a disordered tetrahedral phase (figure 7(b)).

A distinct difference is found in the partial structure factors; $S_{Zn\text{-}Zn}(q)$ shows a broad pre-peak close to $q \simeq 1.3$ Å^{-1}, and $S_{Ca\text{-}Ca}(q)$ a weak shoulder at this momentum transfer (figure 6(c)). The pre-peak exists already in the liquid phase. The Bhatia–Thornton structure factors show that this pre-peak represents a topological short-range order (TSRO)—it appears only in the number-density structure factor $S_{NN}(q)$, and not in the concentration-fluctuation structure factor $S_{cc}(q)$ nor in the cross term $S_{Nc}(q)$ (figure 6(d)). No such pre-peaks have been found in the computer-generated amorphous $CaMg_2$ and $MgZn_2$ phases. We take it as an indication that the structure of the amorphous phase

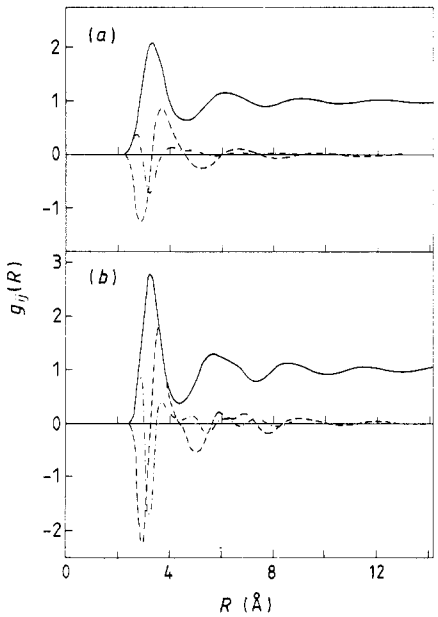

Figure 8. Bhatia–Thornton pair correlation functions for (*a*) liquid and (*b*) amorphous Ca–Zn: NN (——); Nc (– – –); cc (–·–·–).

begins to deviate from the local topology dictated by the principle of tetrahedral close packing.

4.3. CaZn

In the crystalline CaZn compound with the CrB structure, each Zn atom is the centre of a trigonal prism of six Ca atoms. The trigonal prisms are arranged in layers, the Zn atoms forming zigzag chains within these layers (figure 3(*b*)). The peaks in the partial pair correlation functions are in rather good agreement with the inter-atomic distances in the crystal—this holds even for second-neighbour distances (figure 5(*c*)). The partial structure factors have a rather unusual form, especially $S_{Zn-Zn}(q)$; it has an asymmetric main peak (the asymmetry is not unexpected, given the rather large size ratio) and a distinct pre-peak, and the second peak is widely split into two maxima of about equal heights (figure 6(*f*)). Again the origin of the pre-peak is not in CSRO but TSRO as can be seen from the Bhatia–Thornton structure factors (figure 6(*g*)). This is also in agreement with the partial coordination numbers which show only a weak CSRO in both the crystalline and the glassy phases (table 6); compared with a chemically random alloy, 1.5 like neighbours of a Ca atom are exchanged against unlike neighbours, and 2.5 neighbours of a Zn atom in the crystalline phase. For the amorphous phase the corresponding numbers are 0.75 neighbours of a Ca atom and 1.0 neighbour of a Zn atom. Even if the CSRO is rather weak, the Bhatia–Thornton pair correlation functions (figure 8) shows that density and concentration fluctuations are very strongly coupled. The concentration-fluctuation correlation function $g_{cc}(R)$ has the form characteristic for size factor alloys: two peaks separated by a deep minimum, indicating the Zn–Zn, Ca–Zn and Ca–Ca nearest-neighbour shells. The large amplitude of the density–concentration correlation function shows that topological (density fluctuations) and chemical order (concentration fluctuations) are very strongly coupled. In the bond angle distributions the Zn–Zn–Zn angles show the broad peak expected at the Zn-chain angle θ of 112°,

but in addition a peak close to $\theta = 60°$ which is a consequence of the higher number of Zn–Zn neighbours (figure 7(*c*)). The form of $f_{Ca}(\theta)$ of the amorphous phase is compatible with local order similar to that in the CrB phase. The peaks of $f_{Zn}(\theta)$ are shifted to smaller angles compared with the crystalline bond angles—this is a consequence of the overlap of the first peaks in $g_{Ca-Ca}(R)$ and $g_{Ca-Zn}(R)$ (the dominant contribution to $f_{Zn}(\theta)$ comes from Ca–Zn–Ca triplets).

4.4. Ca_3Zn

Essentially the same conclusions can be drawn for the amorphous Ca_3Zn phase; the inter-atomic distances (figure 5(*d*)) and correlation numbers (table 6) of the amorphous phase are very close to those in the crystalline inter-metallic compound, except for a small number of direct Zn–Zn neighbours that are found in the glass but are suppressed in the crystal. In the partial structure factors (figures 6(*h*) and 6(*i*)) and we find again the characteristic pre-peak in $S_{Zn-Zn}(q)$ emphasising a regularity of the Zn–Zn correlations that extends at least to second-neighbour distances, together with the very sharply peaked $S_{Ca-Ca}(q)$ (indicating well defined short-range Ca–Ca correlations). This might be taken as an indication of a topological ordering of local Ca units packed around Zn atoms. To the bond angle distributions the same comments as for CaZn apply; they are compatible with a local trigonal prismatic order, but this is certainly not the only possible interpretation (figure 7(*d*)).

5. Conclusions

We have presented a detailed analysis of the structure of liquid and amorphous Ca–Zn alloys based on molecular dynamics simulations. In the Zn-rich limit the results fit into the pattern characteristic for other simple-metal glasses, the liquid and glassy structures are disordered tetrahedrally close packed. In the Ca-rich phases (Ca_3Zn and CaZn) we find some distinctly different features. The most prominent is the existence of a pre-peak in the Zn–Zn and in the number-density structure factors (it is also reflected as a weak shoulder in $S_{Ca-Ca}(q)$; see figure 6(*c*)) indicating a pronounced *TSRO*. The analysis of the inter-atomic distances, of the coordination numbers and of the bond angle distributions shows that the local order might be described as *trigonal prismatic*, in analogy with the structure of the stable crystalline compounds. In the $CaZn_2$ glass the situation is not so clear cut; evidently this composition corresponds to a transition from trigonal prismatic to tetrahedrally close-packed local order.

Thus from the point of view of their atomic structure the Ca–Zn glasses are intermediate between the simple-metal glasses and the transition-metal glasses (cf § 1). However, the analogy should not be overemphasised; although local trigonal primsatic order exists in both Ca–Zn and transition-metal glasses, the CSRO is weak in Ca–Zn and very strong in transition-metal glasses. We should also emphasise that the connectivity of the trigonal prisms is different in the transition-metal–metalloid compounds of the cementite type [4, 10]. The formation of transition-metal glasses is restricted to a rather narrow composition range; the glass-forming region is very wide in the Ca–Zn system.

Our prediction of a TSRO-induced pre-peak in the structure factors should be easily verifiable by diffraction experiments. We hope that our work will stimulate such measurements.

In the following paper of this series [33], we shall present detailed investigations of the electronic structure of crystalline and amorphous Ca–Zn compounds.

Acknowledgment

This work was supported by the Jubiläumsfonds der Österreichischen Nationalbank under Projects 2991 and 3204.

References

[1] St Amand R and Giessen B C 1978 *Scr. Metall.* **12** 1201
[2] Hafner J 1980 *Phys. Rev.* B **21** 406
[3] Gaskell P H 1978 *Proc. 3rd Int. Conf. Rapidly Quenched Metals* vol. 2, ed. B Cantor (London: Metals Society) p 277
[4] Gaskell P H 1983 *Springer Topics in Applied Physics* vol 53, ed. H Beck and H J Güntherodt (Berlin: Springer) p 5
[5] Fujiwara T 1983 *Springer Series in Solid State Sciences* vol 46, ed. F Yonezawa and T Ninomiya (Berlin: Springer) p 111
[6] Hafner J 1981 *Springer Topics in Applied Physics* vol 46, ed. H J Güntherodt and H Beck (Berlin: Springer) p 93
[7] Frank F C and Kasper J S 1958 *Acta Crystallogr.* **11** 184; 1959 *Acta Crystallogr.* **12** 483
[8] Iandelli A and Palenzona A 1967 *J. Less-Common Met.* **12** 333
[9] Haucke W 1940 *Z. Anorg. (Allg.) Chem.* **244** 17
[10] Pearson W B 1972 *The Crystal Chemistry and Physics of Metals and Alloys* (New York: Wiley–Interscience)
[11] Nelson D R and Sachdev S 1986 *Amorphous Metals and Semiconductors* ed. P Haasen and R I Jaffee (Oxford: Pergamon) p 28
[12] Nelson D R 1985 *Applications of Field Theory to Statistical Mechanics* ed. L Garrido (Berlin: Springer)
[13] Hafner J 1988 *J. Phys. F: Met. Phys.* **18** 153
[14] Jaswal S S and Hafner J 1988 *Phys. Rev.* B **38** 7311
[15] Hafner J and Jaswal S S 1988 *Phys. Rev.* B **38** 7320
[16] Hafner J, Jaswal S S, Tegze M, Pflugi A, Krieg J, Oelhafen P and Güntherodt H J 1988 *J. Phys. F: Met. Phys.* **18** 2583
[17] Heine V and Weaire D 1970 *Solid State Phys.* **24** 247 (New York: Academic)
[18] Hafner J 1986 *Springer Series in Solid State Sciences* vol 70 (Berlin: Springer)
[19] Hansen M and Anderko Z 1958 *Constitution of Binary Alloys* 2nd edn (New York: McGraw-Hill) p 179
[20] Messing A F, Adams M D and Steunenberg R Z 1963 *Trans. Am. Soc. Met.* **56** 345
[21] Fornasini M L, Merlo F and Schubert K 1981 *J. Less-Common Met.* **79** 111
[22] Fornasini M L and Merlo F 1980 *Acta Crystallogr.* B **36** 1739
[23] Schulze G E R and Wieting J 1961 *Z. Metallk.* **52** 743
[24] Fornasini M L 1975 *J. Solid State Chem.* **59** 60
[25] Bruzzone G, Franceschi E and Merlo F 1978 *J. Less-Common Met.* **60** 59
[26] Hafner J and Heine V 1983 *J. Phys. F: Met. Phys.* **13** 2479
[27] Giessen B C, Hong J, Kabacoff L, Polk D E, Raman R and St Amand R 1978 *Rapidly Quenched Metals III* ed. B Cantor (London: Metals Society) p 249
[28] Hafner J 1989 *J. Phys.: Condens. Matter* **1** 1133
[29] Stillinger F H and Weber T A 1985 *Phys. Rev.* B **31** 1954, 5262
[30] Stillinger F H and Weber T A 1984 *J. Chem. Phys.* **80** 4434
[31] Arnold A, Mauser N and Hafner J 1989 *J. Phys.: Condens. Matter* **1** 965
[32] Arnold A and Mauser N *J. Comput. Phys.* submitted
[33] Tegze M and Hafner J 1989 *J. Phys.: Condens. Matter* **1** 8293–303